# SIMPLIFIED NUMERICAL MODEL FOR RAPID DESIGN OF AF MODULE SPRING SHAPE PARAMETERS

**D. S. Liu**

*Department of Mechanical Engineering*
*Advanced Institute of Manufacturing for High-tech Innovations*
*National Chung Cheng University*
*Chiayi, Taiwan*

**C. J. Lu*** **S. H. Chen** **C. S. Liu** **T. W. Liao**

*Department of Mechanical Engineering*
*Advanced Institute of Manufacturing for High-tech Innovations*
*National Chung Cheng University*
*Chiayi, Taiwan*

## ABSTRACT

The autofocusing (AF) performance of cell phone cameras is critically dependent on the design of the voice-coil motor (VCM) used to drive the lens module. Also, the metal springs in the AF module should combine high stiffness with a good actuation response and a light weight. The present study utilizes a reverse engineering approach to construct three-dimensional finite element models of the top and bottom springs in the VCM mechanism. Simulations are then performed to investigate the von Mises stress distribution and stiffness characteristics of the two springs given horizontal and vertical orientations of the AF module, respectively. In performing the simulations, the actuation force is computed using two different analysis methods, namely a simplify structure method and a coupled electromagnetic-structural method. It is shown that the simplify structure method has the advantages of a lower computational complexity and a more comprehensive modeling capability. A further series of simulations is thus to examine the effects of the spring shape parameters on the reaction force developed by the spring stiffness. The results show that the spring stiffness increases with an increasing thickness and a decreasing rib length. The simulation results obtained for different spring shape parameter settings are summarized in the form of a parameter design chart for predicting the reaction force given known values of the spring rib length and spring thickness.

**Keywords:** Autofocus (AF) module, Finite Element Analysis (FEA), Simplify structure method, Coupled electromagnetic-structural method.

## 1. INTRODUCTION

Camera modules are deployed in many portable electronic devices nowadays, most notably in cell phones. Traditionally, such cameras were focused by hand; with the user adjusting the position of the lens manually so as to obtain a sharp image [1]. However, most modern phone cameras are now fitted with sophisticated autofocusing (AF) modules. The literature contains various proposals for power-efficient focusing modules for digital video cameras [2-3]. Furthermore, several Optical Image Stabilization (OIS) systems have been proposed for compensating for the effects of hand-tremble in camcorders [4] or mobile phone devices [5] by shifting the lens or lens group automatically using some form of actuator mechanism. However, in designing AF and OIS systems for mobile phone cameras, maximizing the image quality while simultaneously minimizing the size and weight of the system represents a major challenge.

The problem of miniaturizing the AF module mechanism for cell phone cameras has received extensive attention in the literature [6-8]. However, the related studies lack a detailed investigation into the stiffness and structural characteristics of the AF module components. Modern AF modules for phone camera applications typically employ a voice-coil motor (VCM) to drive the lens group to the required position. However, the metal springs used to stabilize and support the lens module

* Corresponding author (d99420006@ccu.edu.tw)


DOI : 10.1017/jmech.2017.60
Copyright © 2017 The Society of Theoretical and Applied Mechanics
https://doi.org/10.1017/jmech.2017.60 Published online by Cambridge University Press

during actuation must be carefully designed so as to achieve the optimal tradeoff between the structural stiffness of the module, the actuation response, and the physical size and weight of the system.

Accordingly, the present study employs a reverse engineering approach to construct three-dimensional (3D) finite element (FE) models of the top and bottom springs in a commercial cell phone AF module. The FE models are then used in a series of ANSYS simulations to examine the stress distribution and stiffness properties of the springs under typical orientations of the AF module (i.e., horizontal and vertical). The simulations are performed using two different analysis methods, namely a simplify structure method and a coupled electromagnetic-structural method. It is found that while the two methods have a similar accuracy, the simplify structure method has the advantages of a lower computational complexity and an improved modeling capability. Consequently, the simplify structure method is employed to perform a further investigation into the effects of two spring shape parameters (i.e., the rib length and the spring thickness) on the reaction force produced by the springs during actuation. For convenience, the simulation results are summarized in the form of a parameter design chart which enables the reaction force to be predicted given assigned values of the rib length and spring thickness parameters.

## 2. SIMULATION METHODS FOR AF MODULE OPERATION

A typical commercial VCM module is operated using a coil and permanent magnets. We constructed a numerical method, namely a coupled electromagnetic-structural method, to evaluate the stress distribution and stiffness of the top and bottom springs. This method involves using the input current as the actuation force to drive the top and bottom springs and then calculating spring stiffness by coupling the electromagnetic and structure fields. Another analysis method, namely a simplified structure method, was also developed. This method simplifies the numerical model to enhance the comprehensiveness of the model and reduces the simulation's complexity. After comparing the results of the two analysis methods, additional simulations will be performed to examine the effects of spring shape parameters on the reaction force that is developed on the basis of spring stiffness. Finally, the different spring shape parameter settings have been summarized in a parameter design chart for predicting the reaction force given the known values of the spring rib length and spring thickness. Figure 1 presents a flow chart of the numerical analysis and design procedure performed in the present study. This section commences by describing the basic structure of the AF module in a cell phone camera. The details of the two analysis methods used to compute the actuation force for the springs in the AF module are then introduced and discussed.

### 2.1 Auto-Focusing (AF) Module

As described in Section 1, the AF modules in cell phone cameras are generally implemented using some form of VCM device. Figure 2(a) shows the structure of a typical open-loop VCM-based AF module [9]. As shown, the module comprises an arrangement of permanent magnets, a yoke and a fixed base as the fixed part, and a lens module, a lens-holder and a coil as the moving part. The module additionally contains two springs (one top and one bottom) to support and drive the lens module during actuation. Figure 2(b) shows a close-up view of the upper spring in a typical commercial VCM AF module.

### 2.2 Simplify Structure Method

In the simplify structure model, the actuation force acting on the springs is computed directly as the Lorentz force ($F_{VCM}$) produced by the current flowing through the coil in the presence of a magnetic field. In other words, the driving force is computed simply as

$$F_{VCM} = N \cdot I \cdot L \cdot B, \quad (1)[10]$$

where $N$ is the number of coil windings, $I$ is the current passing through the coil, $L$ is the effective length of the coil, and $B$ is the magnetic flux density.

Based on general Hooke's Law equation, the spring stiffness could be calculated by the $F_{VCM}$ and the lens module which is displaced under the effects of the VCM actuation force.

### 2.3 Coupled Electromagnetic-Structural Method

In the electromagnetic-structure coupling model, the electric circuit equation for the AF module is coupled with the magnetic field equation to obtain the actuation force, and the actuation force is then used to compute the spring stiffness. The electric circuit equation is given as

$$J_{en} = \frac{\sigma_e V_n}{2\pi r_n} \quad (2)$$

$$I_n = \int J_n \cdot ds \quad (3)$$

in such a way so as to ensure that the current ($I_n$) in each turn n is identical to the currents in the other turns. Here, $J_{en}$ is the externally-applied current density due to $V_n$, the voltage across each coil turn, $\sigma_e$ is the electrical conductivity, $J_n$ is the current density and s is the surface area of each conductor turn. The average radius of each turn is denoted by $r_n$.

The induced current density in the conductive mobile armature denoted by $J_{i,arm}$ moving with a relative velocity $v$ is given by:

$$J_{i,arm} = \sigma_e (E + v \times B) \quad (4)$$

where $E$ is the electric field and $B$ is the magnetic flux density. As for the stationary base coil, its induced current density reduces to:

$$J_{i,coil} = \sigma_e E \quad (5)$$

The total current density in the coil can be expressed by:



https://doi.org/10.1017/jmech.2017.60 Published online by Cambridge University Press

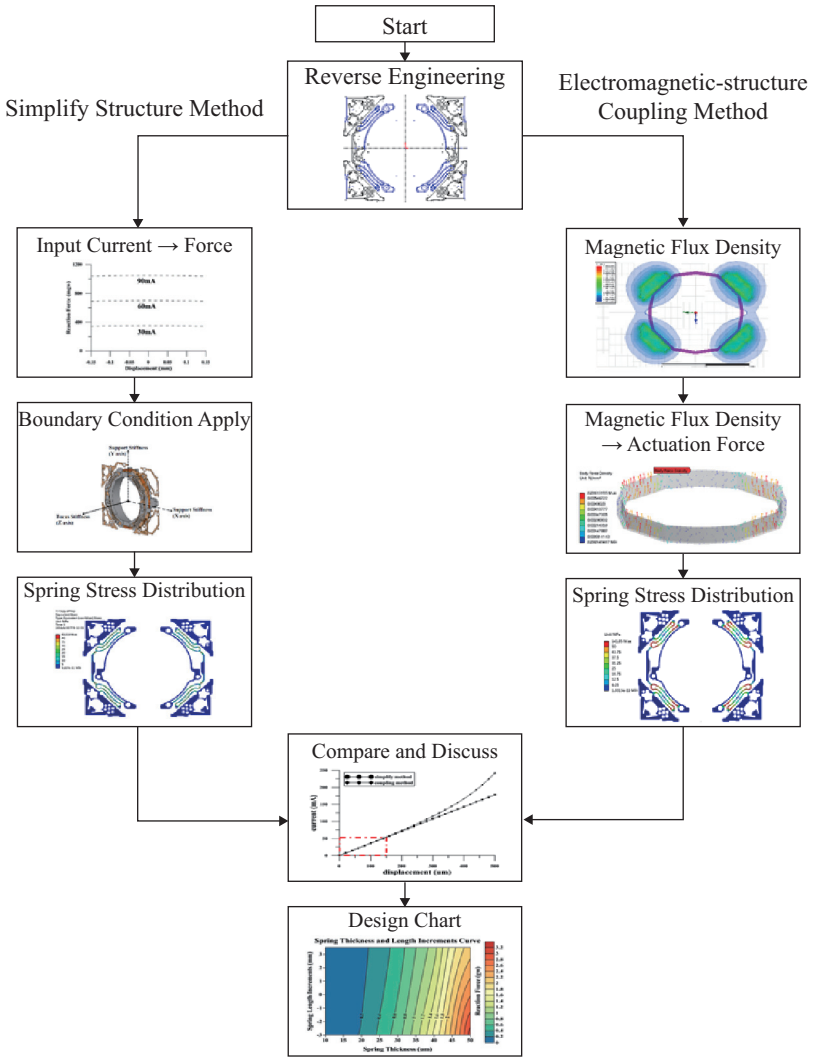



Fig. 1 Flow chart showing numerical analysis and parameter design procedure.

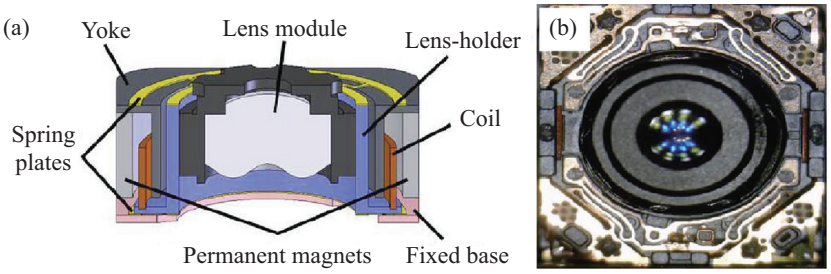



Fig. 2 (a) Typical structure of VCM-based AF module. (b) Photograph of commercial open-loop VCM-based AF module.

$$J_{total} = J_e + J_{i,coil} \tag{6}$$

Based on Maxwell's equations, the magnetic equation for the primary coil can be written as:

$$\sigma_e \frac{\partial A}{\partial t} + \frac{1}{\mu}\nabla \times (\nabla \times A) = J_e \tag{7}$$

where $A$ is the magnetic vector potential, $\nabla$ the nabla operator, $\mu$ the magnetic permeability and $J_e$ the externally-applied current density. The magnetic equation for the mobile armature is given by:

$$\sigma_e \frac{\partial A}{\partial t} + \frac{1}{\mu}\nabla \times (\nabla \times A) - \sigma_e v \times (\nabla \times A) = 0 \tag{8}$$

$$B = \nabla \times A \tag{9}$$

A current in the presence of a perpendicularly-oriented



https://doi.org/10.1017/jmech.2017.60 Published online by Cambridge University Press

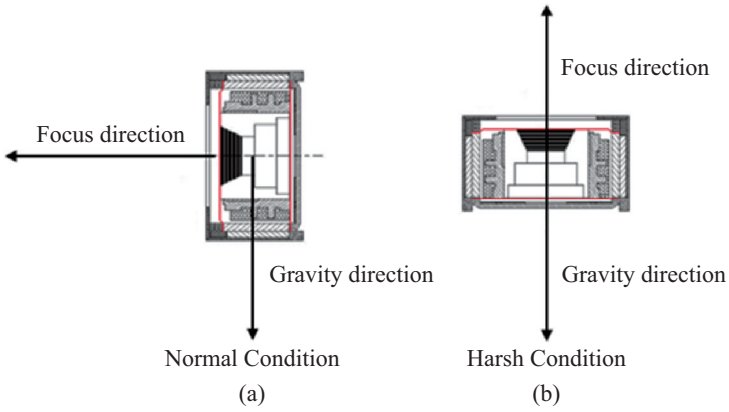



Fig. 3 Operating conditions for AF module: (a) normal condition, and (b) harsh condition.

oriented magnetic field results in a motion force $F_{VCM}$, also known as a Lorentz force, where:

$$F_{VCM} = J_{total} \times B \qquad (10)[11]$$

Note that $F_{VCM}$ would be varied due to the constantly changing distance between lens module and permanent magnets.

### 2.4 Operating Conditions and Loads of AF Module

Figure 3 shows two extreme operating conditions of the AF module. In the first condition, referred to as the normal condition, the module is oriented in the horizontal direction (i.e., perpendicular to the direction of gravity), and hence the top and bottom springs experience no initial deformation (see Fig. 3(a)). However, in the second condition, referred to as the harsh condition, the lens module is oriented in the vertical direction (i.e., parallel to the direction of gravity), and hence the two springs undergo a small initial deformation (see Fig. 3(b)).

When the lens module is displaced under the effects of the VCM actuation force, the springs play a key role not only in driving the module, but also in supporting it and ensuring its dynamic stability. As a result, the stiffness of the two springs is an important concern. In practice, two different stiffness properties should be considered, namely the support stiffness and the focus stiffness. As shown in Fig. 4, the support stiffness provides the force required to prevent the lens module from deviating from the central focus axis during forward and backward motion. By contrast, the focus stiffness provides the actual driving force needed to translate the lens module in the forward and reverse directions. The boundary conditions and loads described in this section are applied in both analysis models.

## 3. FINITE ELEMENT MODELS OF AF MODULE SPRINGS

For a commercial VCM unit, the correlation between the coil displacement and the winding current is readily determined from the specification. However, the stiffness properties of the springs are not included in the spec. Moreover, due to the small size and high fragility of the springs, it is difficult to measure their stiffness properties experimentally. Nonetheless, for a designer, the spring stiffness is an important concern since it determines the weight of the lens module which can be supported/driven by the VCM module. Accordingly, as described below, this study employed a reverse engineering approach to construct 3D models of the top and bottom springs in a commercial VCM AF module such that the relationship between the spring shape parameters and the spring stiffness could then be explored through numerical simulations.

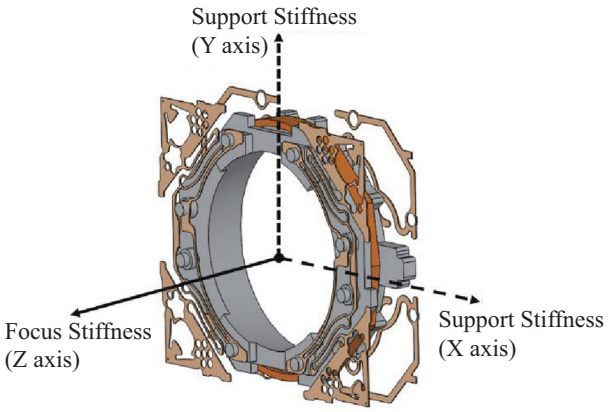



Fig. 4 Support stiffness and focus stiffness of VCM AF module springs.

The springs in the AF module were observed through an optical microscope (Nikon Eclipse LV100). The images were captured in a digital form using Image-Pro Premier software, as shown in Fig. 5.

The digital images were converted into 3D digital models using SolidWorks software (see Fig. 6). The models were then imported into ANSYS to construct corresponding numerical models, as shown in Fig. 7. The FE models were used in a series of simulations based on the coupled electromagnetic-structural method and simplify structure method, respectively, to investigate the stress distribution and stiffness properties of the two springs. In the coupled electromagnetic-structural



https://doi.org/10.1017/jmech.2017.60 Published online by Cambridge University Press

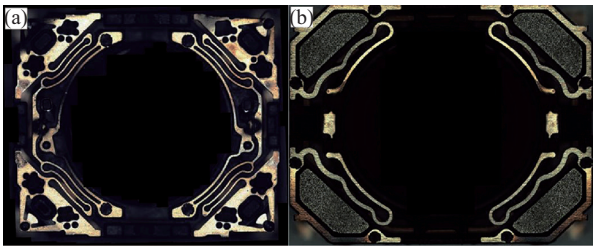



Fig. 5 Digital images of (a) top spring and (b) bottom spring in VCM AF module.

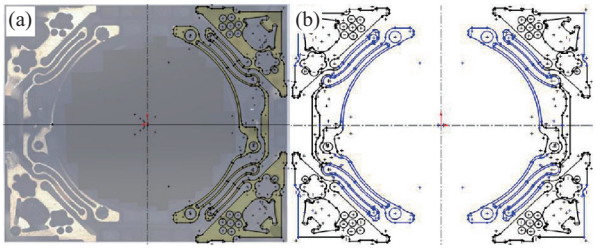



Fig. 6 Conversion of digital image of top spring to digital model.

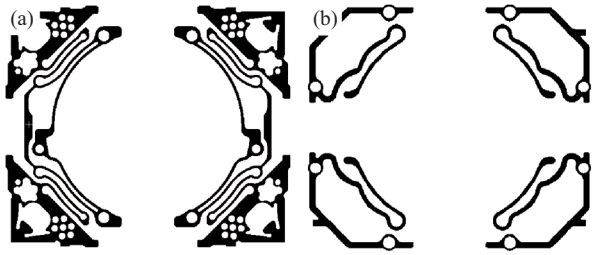



Fig. 7 Numerical models of: (a) top spring, and (b) bottom spring.

method, the magnetic flux responsible for generating the actuation force was produced by four permanent magnets arranged evenly around the circumference of the VCM coil. The displacement of the lens module caused by the magnetic flux was then applied to the top and bottom springs in order to calculate the resulting stress distribution and deformation. In the simplify structure method, the actuation force, $F_{VCM}$, was modeled simply as a uniform load acting on the two springs. For both analysis methods, the boundary conditions were assigned in accordance with the technical specification of the considered AF module. Because the springs must be strong enough to keep the lens on the focus axis, the allowable deformation of the springs in the X- and Y-directions should be limited. In analyzing the support stiffness, the maximum allowable displacement of the lens module in the X- and Y-directions was set to 0.01 mm, while that in the Z-direction was set to 0 mm. On the basis of the limited rib length and the maximum allowable actuation distance of the focus axis from commercial specifications, in analyzing the focus stiffness, the maximum allowable displacement of the lens module in the Z-direction was

Table 1 Parameters used in AF module simulations.

| Variable | Parameter appellation/value |
|---|---|
| Permanent magnet material | Nd-Fb-B N48H |
| Dimensions of permanent magnets | 2.94 × 0.9 × 1.54 mm |
| Radius/thickness of coil | 3.83/0.71 mm |
| Number of coil windings | 52 turns |
| Gap between coil and magnets | 0.12 mm |
| Coercivity of permanent magnets | 1008008 A/m |
| Remanence of permanent magnets | 1.05 T |
| Spring material | C19900HP-GSH |
| Spring elastic modulus | 127 GPa |
| Spring density | 8.7 g/cm$^3$ |
| Spring yield stress | 1390 MPa |

set to 0.15 mm, whereas those of the X- and Y- directions were set to 0 mm. Moreover, the weight of the lens module was set as 144.6 mgw in accordance with the manufacturer's spec, and the overall dimensions of the top and bottom springs were set as 9.32 × 7.8 × 0.03 mm and 9.8 × 8.34 × 0.03 mm, respectively. Finally, both springs were assumed to be fabricated of C19900HP-GSH titanium copper alloy. All of the parameters and material properties used in the simulations are summarized in Table 1.

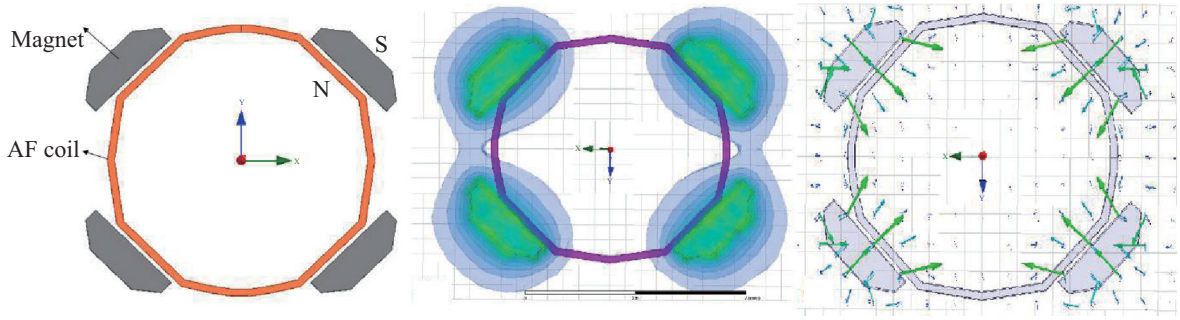
## 4. SIMULATION RESULTS

In performing the coupled electromagnetic-structural simulations, the permanent magnets were assumed to be deployed as shown in Fig. 8(a). The corresponding magnetic flux density distribution thus had the form shown in Fig. 8(b). As shown, the magnetic flux density is non-uniformly distributed around the circumference of the coil. Fig. 8(c) shows the magnetic flux simulation result was consistent with the direction of magnetic flux which was produced by the permanent magnets. Given a knowledge of this magnetic flux, the actuation force acting on the lens module can be computed simply as the Lorentz force.

In accordance with basic electromagnetic theory, the actuation force induced by the four magnets shown in Fig. 8(a) acts in the Z-direction (i.e., the translation direction of the lens assembly). Consequently, the coupled electromagnetic-structural method enables the focus stiffness of the top and bottom springs to be estimated. However, since the arrangement of the four magnets is fixed in the simulations, the support stiffness (in which the displacement of the lens module in the X- and Y-directions is of interest) cannot be determined. By contrast, in the simplify structure method, both the focus stiffness and the support stiffness of the two springs can be estimated since the actuation force, $F_{VCM}$, is modeled simply as a uniform load. In other words, of the two methods, the simplify structure method provides a more comprehensive modeling capability. For example, as shown in Fig. 9(a), the maximum stress in the bottom

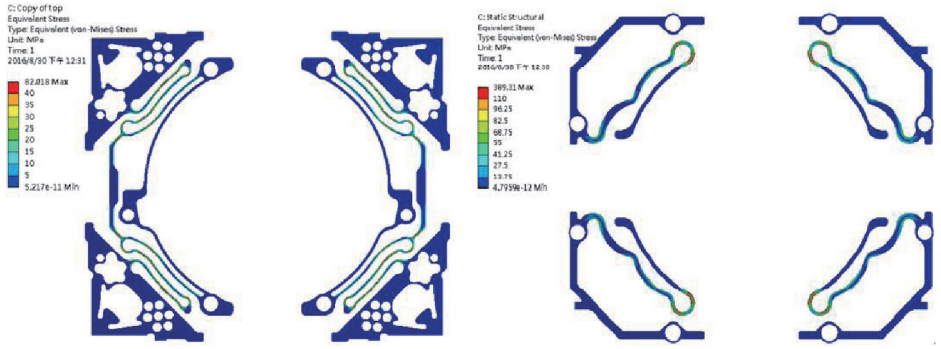


https://doi.org/10.1017/jmech.2017.60 Published online by Cambridge University Press



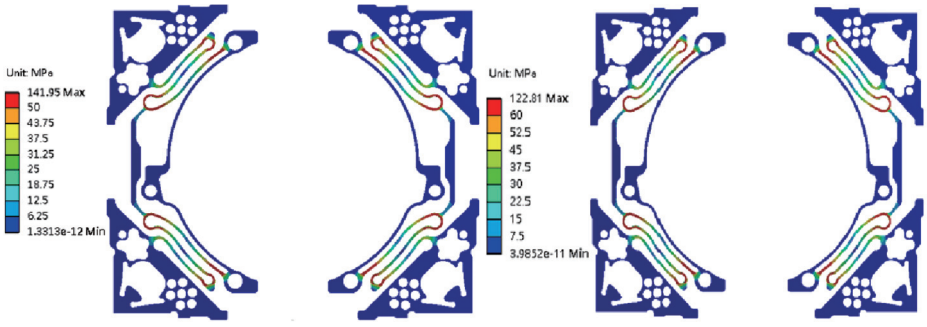

(a) (b) (c)

Fig. 8 (a) AF coil and permanent magnet locations, (b) magnetic flux density distribution, and (c) magnetic flux direction.



(a) (b)

Fig. 9 Results obtained using simplified structure method for von Mises stress distribution in: (a) top spring, and (b) bottom spring in support stiffness condition.




(a) (b)

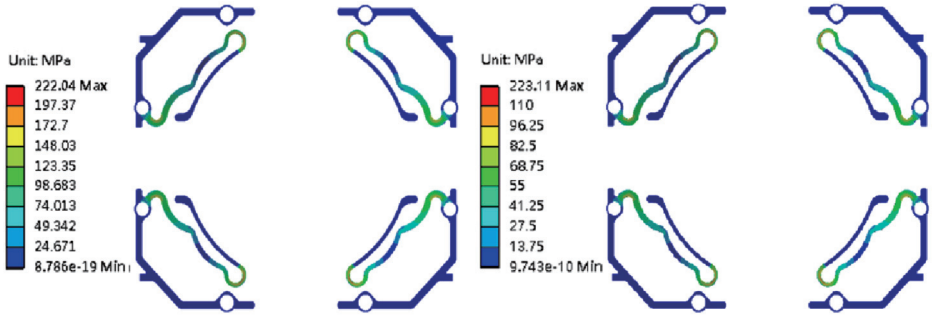
Fig. 10 Results obtained for von Mises stress distribution in top spring in focus stiffness condition by: (a) coupled electromagnetic-structural method, and (b) simplify structure method.

spring in the support stiffness condition is estimated by the simplify structure method to be 82.0 MPa, while that in the bottom spring is estimated to be 389.3 MPa (see Fig. 9(b)).

Figures 10 and 11 show the results obtained by the coupled electromagnetic-structural method and simplify structure method, respectively, for the von Mises stress distributions in the top and bottom spring in the focus stiffness condition. As shown in Fig. 10(a), the maximum stress calculated by the coupled electromagnetic-structural method is equal to 141.9 MPa. Similarly, the maximum stress calculated by the simplify structure method is 122.8 MPa (see Fig. 10(b)). For the bottom spring, the maximum stress in the focus stiffness condition is estimated to be 222.0 MPa by the coupled electromagnetic-structural method (see Fig. 11(a)) and 223.1 MPa by the simplify structure method (see Fig. 11(b)). Overall, the results presented in Figs. 10 and 11 show that the two analysis methods yield similar results for the maximum stress value and stress distribution in



https://doi.org/10.1017/jmech.2017.60 Published online by Cambridge University Press




(a) (b)

Fig. 11 Results obtained for von Mises stress distribution in bottom spring in focus stiffness condition by: (a) coupled electromagnetic-structural method, and (b) simplify structure method.

Table 2 Results obtained by two analysis methods for stiffness values of top and bottom springs in focus and support stiffness conditions.

| | Focus stiffness (mgw/mm) | Support stiffness (mgw/mm) |
|---|---|---|
| Top Spring (coupling) | 260.63 | -- |
| Top Spring (simplify) | 244.1 | 1819.3 |
| Bottom Spring (coupling) | 389.31 | -- |
| Bottom Spring (simplify) | 364.62 | 11032 |

the two springs.

It is noted that all six stress values are far lower than the yield stress of the spring material (i.e., 1390 MPa, see Table 1). Table 2 shows the results obtained by the two calculation methods for the stiffness values of the top and bottom springs in the two stiffness conditions. Note that in the actuation process, the stiffness represents the reaction force applied by the springs. Observing the results presented in Table 2, it is seen that the reaction force provided by the bottom spring is significantly higher than that provided by the top spring for both conditions. In other words, the reaction force increases as the complexity of the spring design decreases (see Figs. 5(a) and 5(b) for comparison purposes).

Figure 12 shows the results obtained by the two analysis methods for the relationship between the coil current and the lens module displacement in the focus condition. Note that the area indicated by the bold dotted lines represents the operational range of the considered commercial AF module (as determined from the manufacturer's spec). For lower values of the lens displacement, a good agreement is observed between the results obtained by the two methods. However, for focus displacement values greater than 200 μm, a significant discrepancy between the two sets of results emerges. More specifically, the displacement continues to increases linearly with an increasing current in the simplify structure method, but increases almost exponentially in the coupled electromagnetic-structural method. However, within the usual operation range of the VCM motor,

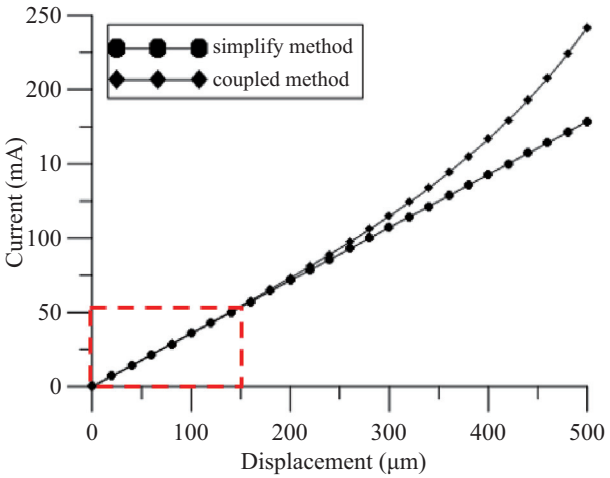
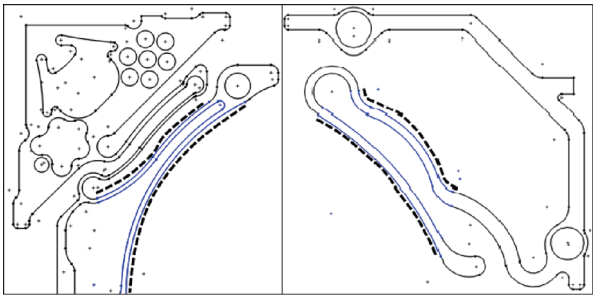



Fig. 12 Results obtained by two analysis methods for relationship between coil current and lens module displacement in focus condition.



(a) (b)

Fig. 13 (a) Spring rib length increment range for top spring, and (b) spring rib length increment range for bottom spring.

the two methods produce very similar results and hence, for reasons of computational convenience, the remaining analyses are performed using the simplify structure method.

A further series of simulations was performed to investigate the effects of two spring shape parameters, namely the spring rib length (see Fig. 13) and the spring



https://doi.org/10.1017/jmech.2017.60 Published online by Cambridge University Press

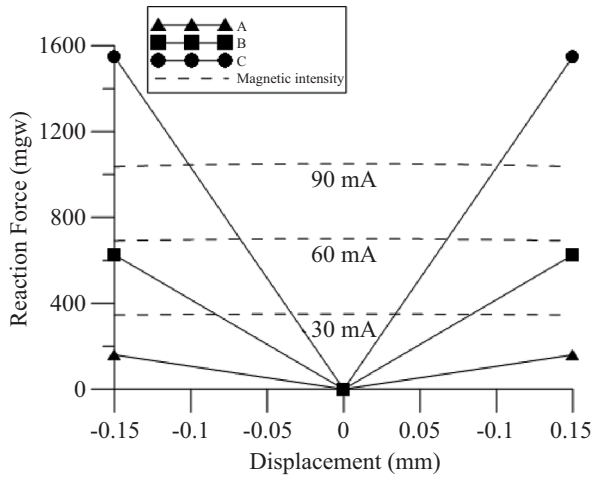



Fig. 14 Combined focus stiffness behavior of bop and bottom springs in normal operating condition for three different settings of spring shape parameters.

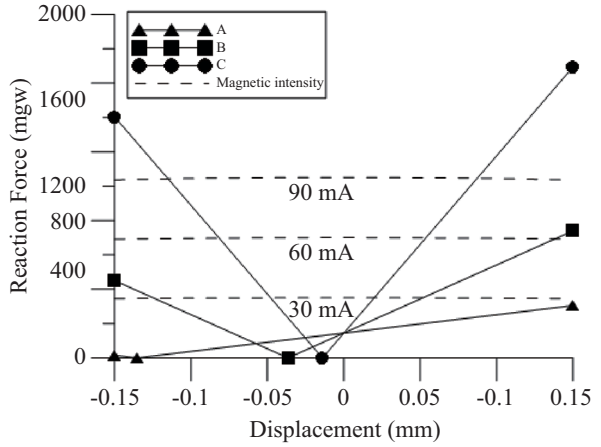



Fig. 15 Combined focus stiffness behavior of bop and bottom springs in harsh operating condition for three different settings of spring shape parameters.

thickness, on the spring stiffness (i.e., reaction force). For both springs (i.e., top and bottom), the simulations considered spring thickness values in the range of 10 to 50 μm and rib length increments in the range of -3.0 to +3.5 mm. Note that a rib length increment of 0 represents the length of the rib in the original FE model. Moreover, the bold dotted lines in Fig. 13 show the variation range of the spring rib length increment in the top and bottom springs.

Figures 14 and 15 shows the simulation results obtained for the combined focus stiffness (i.e., total reaction force) of the two springs given three illustrative settings of the spring rib length and spring thickness parameters (see Table 3) and two operating conditions of the AF module (i.e., normal and harsh, respectively). Note that the dotted lines in the two figures show the $F_{VCM}$ force of the modeled VCM (as determined from the

Table 3 Illustrative spring shape parameter settings used in focus stiffness analyses.

| | Rib Length Increment (mm) | Thickness (um) | Stiffness (mgw/mm) |
|---|---|---|---|
| A | 2 | 20 | 1067.3 |
| B | 0 | 30 | 3965.1 |
| C | -2 | 40 | 10323.8 |

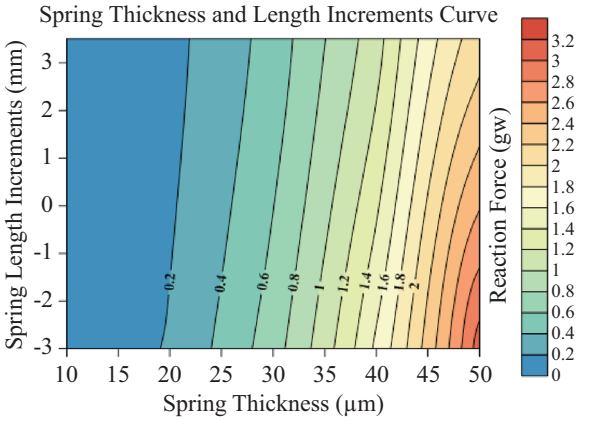



Fig. 16 Parameter design chart for combined spring focus stiffness.

manufacturer's spec) given input currents of 30 mA, 60 mA and 90 mA, respectively. As expected, for both operating conditions, the reaction force is positively correlated with the spring thickness, but negatively correlated with the rib length. Figure 15 additionally shows that in the harsh operating mode, a higher value of the focus stiffness is beneficial in reducing the initial deformation of the springs. Conversely, the initial deformation of the springs increases as the focus stiffness reduces. Notably, however, while a higher focus stiffness reduces the initial deformation, the driving force required to actuate the lens assembly may exceed the maximum $F_{VCM}$ output of the VCM device. For example, as shown Figs. 14 and 15, the driving force required to achieve the maximum displacement value (0.15 mm) given the Case C spring design is higher than the maximum $F_{VCM}$ output available from the VCM irrespective of the operating condition (normal or harsh) employed.

Figure 16 summarizes the simulation results obtained for the combined reaction force of the springs given different values of the spring length increment and spring thickness. The chart provides a simple and convenient means of predicting the reaction force for any given values of the two spring shape parameters within the respective ranges.

## 5. CONCLUSIONS

This study has investigated the support stiffness and focus stiffness properties of a commercial VCM-based



https://doi.org/10.1017/jmech.2017.60 Published online by Cambridge University Press

autofocusing camera module using two different analysis methods, namely a coupled electromagnetic-structural method and a simplify structure method. A reverse engineering technique has been employed to construct 3D FE models of the top and bottom springs in the VCM module. ANSYS FE simulations have then been performed to evaluate the von Mises stress distribution within the two springs and to explore the effects of the spring rib length and spring thickness parameters on the developed reaction force. The main contributions and findings of this study can be summarized as follows.

1. 3D FE numerical models have been constructed of the top and bottom springs in a commercial VCM module used for AF/OIS purposes in a cell phone camera. The validity of the models has been ensured by employing a reverse engineering technique to capture the exact size and configuration of the springs used in the VCM module.
2. Two different analysis models have been proposed for evaluating the reaction force acting on the lens module during actuation, namely a coupled electromagnetic-structural model and a simplify structure model. A good agreement has been observed between the results obtained from the two methods for the von Mises stress distribution within the top and bottom springs. However, the coupled electromagnetic-structural method involves a more complex calculation process. Moreover, it cannot estimate the spring stiffness in the support stiffness condition since the positions of the permanent magnets in the VCM device are fixed in the present simulations. Thus, the simplify structure method provides a simpler and more comprehensive approach for modeling the focus and stiffness properties of the VCM springs.
3. The simulation model can be applied to find the results have shown that the spring stiffness increases with an increasing spring thickness and a decreasing rib length. Moreover, as the focus stiffness increases, the initial deformation of the top and bottom springs decreases. As a result, a more stable actuation performance is achieved. However, given a large focus stiffness, the power required to drive the lens module to the point of maximum displacement may exceed that which can be provided by the VCM AF module. It is provide the developer a design viewpoint to prevent wasting battery and increasing the performance of AF from the shape factor relationship.
4. A parameter design chart has been constructed to visualize the effects of the spring rib length and spring thickness parameters on the reaction force developed by the springs in the VCM AF module. The chart provides a convenient tool for predicting the reaction force produced by the two springs given prescribed values of the spring rib length and thickness.

The present study has focused specifically on a commercial VCM AF module in which the top and bottom springs have dimensions of 9.32 × 7.8 × 0.03 mm and 9.8 × 8.34 × 0.03 mm, respectively. However, the reverse engineering technique and numerical modeling approach employed in the study can be equally applied to any VCM-based AF module used in commercial cell phone cameras.

## ACKNOWLEDGEMENTS

The current authors gratefully acknowledge the financial support provided to this study by the Ministry of Science and Technology, Taiwan, ROC, under Grant Nos. MOST 103-2221-E-194-010-MY3 and MOST 104-2221-E-194-001-MY3.

## REFERENCES

1. Sohn, S. M. *et al*., "Soc Design of an Auto-Focus Driving Image Signal Processor for Mobile Camera Applications," *IEEE Transactions on Consumer Electronics*, **52**, pp. 10-16 (2006).
2. Yu, H. C. *et al*., "Design of a Voice Coil Motor Used in the Focusing System of a Digital Video Camera," *IEEE Transactions on Magnetics*, **41**, pp. 3979-3981 (2005).
3. Yu, H. C. *et al*., "Low Power Consumption Focusing Actuator for a Mini Video Camera," *Journal of Applied Physics*, DOI: 10.1063/1.2158927 (2006).
4. Kusaka, H., Tsuchida, Y. and Shimohata, T., "Control Technology for Optical Image Stabilization," *SMPTE Motion Imaging Journal*, **111**, pp. 609-615 (2002).
5. Song, M. G. *et al*., "Development of Small Sized Actuator with Compliant Mechanism for Optical Image Stabilization," *IEEE Transactions on Magnetics*, **46**, pp. 2369-2372 (2010).
6. Chung, M. J. and Son, S. Y., "Development of Compact Auto Focus Actuator for Camera Phone by Applying New Electromagnetic Configuration," *Journal of Mechanical Science and Technology*, **20**, pp. 2087-2093 (2006).
7. Chao, P. C. P., Chiu, C. W., Liang, H. K. and Kao, N. Y. Y., "Intelligent Actuation Strategy Via Image Feedbacks for a Magnetically Actuated Autofocusing Module in Mobile Phones," *Journal of Applied Physics*, DOI: 10.1063/1.2835451 (2008).
8. Liu, C. S. *et al*., "Design and Characterization of Miniature Auto-Focusing Voice Coil Motor Actuator for Cell Phone Camera Applications," *IEEE Transactions on Magnetics*, **45**, pp. 155-159 (2009).
9. Liu, C. S. and Lin, P. D., "A Miniaturized Low-Power VCM Actuator for Auto-Focusing Applications," *Optics Express*, **16**, pp. 2533-2540 (2008).



https://doi.org/10.1017/jmech.2017.60 Published online by Cambridge University Press

10. Chiu, C. W., Chao, P. C. P. and Wu, D. Y., "Optimal Design of Magnetically Actuated Optical Image Stabilizer Mechanism for Cameras in Mobile Phones Via Genetic Algorithm," *IEEE Transactions on Magnetics*, **43**, pp. 2582-2584 (2007).
11. Bissal, A., Eriksson, A., Magnusson, J. and Engdahl, G., "Hybrid Multi-Physics Modeling of an Ultra-Fast Electro-Mechanical Actuator," *Actuators*, **4**, pp. 314-335 (2015).

(Manuscript received April 25, 2017,
accepted for publication June 5, 2017.)



https://doi.org/10.1017/jmech.2017.60 Published online by Cambridge University Press